High-precision photometry by telescope defocussing. IV. Confirmation of the huge radius of WASP-17 b[⋆]

John Southworth [1], M. Dominik [2]†, X.-S. Fang [3], K. Harpsøe [4,5], U. G. Jørgensen [4,5],
E. Kerins [6], C. Liebig [2], L. Mancini [7,8], J. Skottfelt [4,5], D. R. Anderson [1], B. Smalley [1],
J. Tregloan-Reed [1], O. Wertz [9], K. A. Alsubai [10], V. Bozza [8,11,12], S. Calchi Novati [8,11],
S. Dreizler [13], S.-H. Gu [3], T. C. Hinse [14], M. Hundertmark [2,13], J. Jessen-Hansen [15,16],
N. Kains [17], H. Kjeldsen, [15] M. N. Lund [15], M. Lundkvist [15], M. Mathiasen [4], M. T.
Penny [6,18], S. Rahvar [19,20], D. Ricci [9], G. Scarpetta [8,11,12], C. Snodgrass [21], J. Surdej [9],

[1] *Astrophysics Group, Keele University, Staffordshire, ST5 5BG, UK*
[2] *SUPA, University of St Andrews, School of Physics & Astronomy, North Haugh, St Andrews, KY16 9SS, UK*
[3] *National Astronomical Observatories/Yunnan Observatory, Chinese Academy of Sciences, Kunming 650011, China*
[4] *Niels Bohr Institute, University of Copenhagen, Juliane Maries vej 30, 2100 Copenhagen Ø, Denmark*
[5] *Centre for Star and Planet Formation, Natural History Museum of Denmark, University of Copenhagen, øster Voldgade 5-7, 1350 Copenhagen K, Denmark*
[6] *Jodrell Bank Centre for Astrophysics, University of Manchester, Oxford Road, Manchester M13 9PL, UK*
[7] *Max Planck Institute for Astronomy, Königstuhl 17, 69117 Heidelberg, Germany*
[8] *Istituto Internazionale per gli Alti Studi Scientifici (IIASS), 84019 Vietri Sul Mare (SA), Italy*
[9] *Institut d'Astrophysique et de Géophysique, Université de Liège, 4000 Liège, Belgium*
[10] *Qatar Foundation, Doha, Qatar*
[11] *Dipartimento di Fisica "E. R. Caianiello", Università di Salerno, Via Ponte Don Melillo, 84084-Fisciano (SA), Italy*
[12] *Istituto Nazionale di Fisica Nucleare, Sezione di Napoli, Napoli, Italy*
[13] *Institut für Astrophysik, Georg-August-Universität Göttingen, Friedrich-Hund-Platz 1, 37077 Göttingen, Germany*
[14] *Korea Astronomy and Space Science Institute, Daejeon, Republic of Korea*
[15] *Stellar Astrophysics Centre (SAC), Department of Physics and Astronomy, Aarhus University, Ny Munkegade 120, DK-8000 Aarhus C, Denmark*
[16] *Nordic Optical Telescope, Apartado 474, E-38700 Santa Cruz de La Palma, Spain*
[17] *European Southern Observatory, Karl-Schwarzschild-Straße 2, 85748 Garching bei München, Germany*
[18] *Department of Astronomy, Ohio State University, 140 W. 18th Ave., Columbus, OH 43210, USA*
[19] *Department of Physics, Sharif University of Technology, P. O. Box 11155-9161 Tehran, Iran*
[20] *Perimeter Institute for Theoretical Physics, 31 Caroline Street North, Waterloo, Ontario N2L 2Y5, Canada*
[21] *Max-Planck-Institute for Solar System Research, Max-Planck Str. 2, 37191 Katlenburg-Lindau, Germany*

8 February 2013

ABSTRACT

We present photometric observations of four transits in the WASP-17 planetary system, obtained using telescope defocussing techniques and with scatters reaching 0.5 mmag per point. Our revised orbital period is 4.0 ± 0.6 s longer than previous measurements, a difference of 6.6σ, and does not support the published detections of orbital eccentricity in this system. We model the light curves using the JKTEBOP code and calculate the physical properties of the system by recourse to five sets of theoretical stellar model predictions. The resulting planetary radius, $R_{\rm b} = 1.932 \pm 0.052 \pm 0.010 \, {\rm R_{Jup}}$ (statistical and systematic errors respectively), provides confirmation that WASP-17 b is the largest planet currently known. All fourteen planets with radii measured to be greater than $1.6 \, {\rm R_{Jup}}$ are found around comparatively hot ($T_{\rm eff} > 5900 \, {\rm K}$) and massive ($M_{\rm A} > 1.15 \, {\rm M_\odot}$) stars. Chromospheric activity indicators are available for eight of these stars, and all imply a low activity level. The planets have small or zero orbital eccentricities, so tidal effects struggle to explain their large radii. The observed dearth of large planets around small stars may be natural but could also be due to observational biases against deep transits, if these are mistakenly labelled as false positives and so not followed up.

Key words: stars: planetary systems — stars: fundamental parameters — stars: individual: WASP-17

---

1   INTRODUCTION

Ongoing surveys for transiting extrasolar planets (TEPs) have detected an unexpectedly diverse set of objects, such as HD 80606 b, a massive planet on an extremely eccentric orbit ($e = 0.9330 \pm 0.0005$; Hébrard et al. 2010); super-Earths on very short-period orbits like CoRoT-7 b and 55 Cnc e (Léger et al. 2009; Winn et al. 2011); WASP-18 b with a mass of $10\,\mathrm{M_{Jup}}$ and an orbital period of 0.94 d (Hellier et al. 2009); WASP-33 b, a very hot planet revolving around a metallic-lined pulsating A star (Collier Cameron et al. 2010); a system of six planets transiting the star Kepler-11 (Lissauer et al. 2011); and a planet orbiting the eclipsing binary star system Kepler-16 (Doyle et al. 2011).

Among these objects, WASP-17 b stands out as both the largest known planet and the first found to follow a retrograde orbit (Anderson et al. 2010, hereafter A10). However, the reliability of its radius measurement was questionable for two reasons. Firstly, it rested primarily on a single high-quality transit light curve, whereas it is widely appreciated that correlated noise can afflict individual light curves whilst remaining undetectable in isolation (e.g. Gillon et al. 2007; Adams et al. 2011). Correlated noise is clearly visible in the residuals of the best-fitting model for this transit (fig. 2 in A10). Secondly, the orbital eccentricity, e, was poorly constrained, and this uncertainty in the orbital velocity of the planet has major implications for the interpretation of the transit light curves.

The WASP-17 discovery paper (A10) presented three measurements of the planetary radius, R_{b}, based on models with different assumptions. The preferred model (Case 1) was a straightforward fit to the available data, yielding $R_{\mathrm{b}} = 1.74^{+0.26}_{-0.23}\,\mathrm{R_{Jup}}$ and $e = 0.129^{+0.106}_{-0.068}$. The test of Lucy & Sweeney (1971), which accounts for the fact that a measured eccentricity is a biased estimator of the true value, indicates a probability of only 83% that this eccentricity is significant. Case 2 incorporated a Bayesian prior on the stellar mass and radius to encourage them towards a solution appropriate for a main-sequence star, and resulted in $R_{\mathrm{b}} = 1.51 \pm 0.10\,\mathrm{R_{Jup}}$ and $e = 0.237^{+0.068}_{-0.069}$. The third and final model, Case 3, did not use the main-sequence prior but instead enforced $e = 0$, and yielded $R_{\mathrm{b}} = 1.97 \pm 0.10\,\mathrm{R_{Jup}}$. The measured size of the planet is clearly very sensitive to the treatment of orbital eccentricity.

Triaud et al. (2010) and Bayliss et al. (2010) subsequently confirmed the provisional finding that WASP-17 b has a retrograde orbit, from radial velocity observations obtained during transit. Triaud et al. (2010) also obtained improved spectroscopic parameters for the host star. They assumed $e = 0$ and found $R_{\mathrm{b}} = 1.986^{+0.089}_{-0.074}\,\mathrm{R_{Jup}}$. Wood et al. (2011) have detected sodium in the atmosphere of WASP-17 b, using échelle spectroscopy obtained outside and during transit.

Anderson et al. (2011, hereafter A11) used an alternative method to constrain the orbital shape of the WASP-17 system: measurements of the time of occultation of the planet by the star in infrared light curves obtained by the *Spitzer* satellite. To first order, the orbital phase of secondary eclipse (occultation) depends on the product $e\cos\omega$ where ω is the longitude of periastron (Kopal 1959). A11 obtained $e\cos\omega = 0.00352 \pm 0.00075$ and $e = 0.028^{+0.015}_{-0.018}$, finding $e\cos\omega$ to be significantly different from zero at the 4.8σ level. Inclusion of the *Spitzer* data, alongside existing observations, led to the measurement $R_{\mathrm{b}} = 1.991 \pm 0.081\,\mathrm{R_{Jup}}$. This was achieved without making assumptions about e or ω, so represents the first clear demonstration that WASP-17 b is the largest planet with a known radius. One remaining concern was that the orbital ephemeris of the system had to be extrapolated to
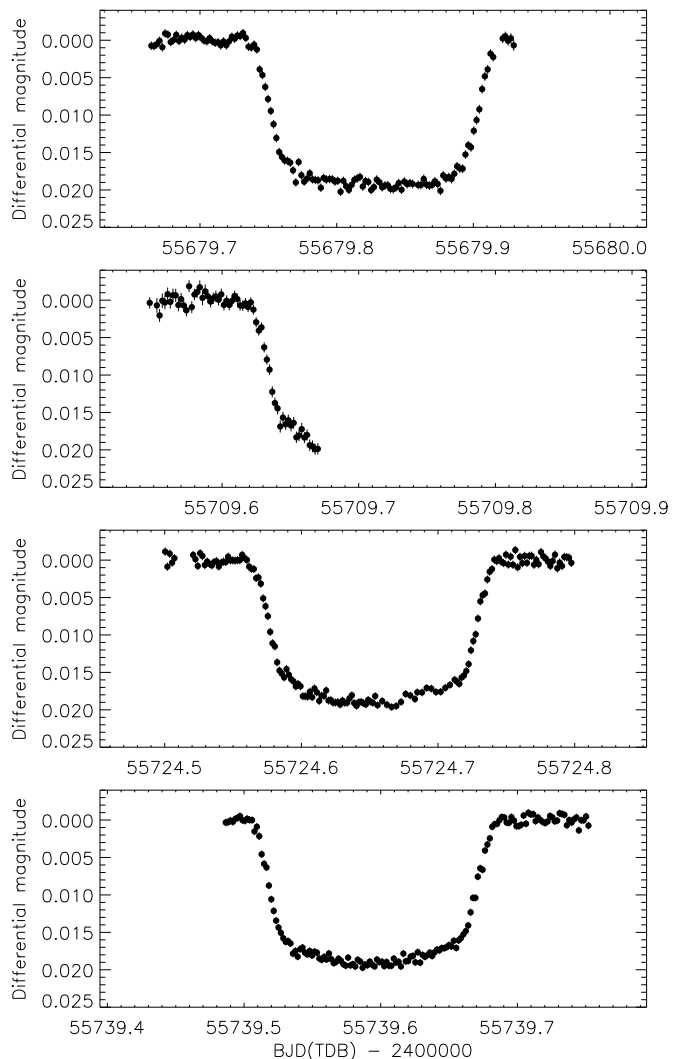

Figure 1. Light curves of WASP-17. The error bars have been scaled to give $\chi^2_\nu = 1.0$ for each night, and in some cases are smaller than the symbol sizes.

the times of the *Spitzer* observations, potentially compromising the measurement of the phase of mid-occultation and therefore $e\cos\omega$.

In this work we present new photometry of three complete transits of WASP-17 b, obtained using telescope-defocussing techniques. These lead to a refinement of the orbital ephemeris, shedding new light on the possibility of orbital eccentricity in this system. They also allow a new set of physical properties of the system to be obtained, which are more precise and no longer dependent on the quality of a single follow-up light curve. We use these data to confirm the standing of WASP-17 b as the largest known planet, at $R_{\mathrm{b}} = 1.932 \pm 0.053\,\mathrm{R_{Jup}}$.

2   OBSERVATIONS AND DATA REDUCTION

We observed four transits of WASP-17 through a Bessell R filter, in the 2011 observing season, using the 1.54 m Danish Telescope[1]

Table 1. Log of the observations presented in this work. N_{obs} is the number of observations and 'Moon illum.' is the fractional illumination of the Moon at the midpoint of the transit.

Transit	Date of first obs	Start time (UT)	End time (UT)	N_{obs}	Exposure time (s)	Filter	Airmass	Moon illum.	Aperture radii (px)	Scatter (mmag)
1	2011 04 28	03:48	10:10	128	120	R	$1.19 \rightarrow 1.00 \rightarrow 1.57$	0.212	32, 46, 65	0.560
2	2011 05 28	00:58	03:55	63	120	R	$1.31 \rightarrow 1.01$	0.199	28, 38, 58	0.762
3	2011 06 11	23:51	06:51	152	100	R	$1.46 \rightarrow 1.00 \rightarrow 1.48$	0.826	30, 42, 60	0.528
4	2011 06 26	23:32	05:54	152	100	R	$1.26 \rightarrow 1.00 \rightarrow 1.45$	0.184	30, 40, 60	0.475

Table 2. Excerpts of the light curve of WASP-17. The full dataset will be made available at the CDS.

BJD(TDB)	Diff. mag.	Uncertainty
55679.66520	0.000732	0.000572
55679.93036	0.000675	0.000721
55709.54791	0.000352	0.000761
55709.67092	0.019863	0.000766
55724.50116	-0.001133	0.000560
55724.79836	0.000359	0.000568
55739.48740	0.000324	0.000508
55739.75282	0.000740	0.000499

at ESO La Silla, Chile (Table 1). Our approach was to defocus the telescope and use relatively long exposure times of 100–120 s (see Southworth et al. 2009a,b). This technique results in a higher observing efficiency, as less time is spent on reading out the CCD, and therefore lower Poisson and scintillation noise. It also greatly decreases flat-fielding noise as several thousand pixels are contained in each point spread function (PSF), and makes the results insensitive to any changes in the seeing during an observing sequence. We autoguided throughout each sequence in order to keep the PSFs on the same CCD pixels, which reduces any remaining susceptibility to flat-fielding noise. The second of the observing sequences suffered from clouds from shortly before the midpoint to after the end of the transit, and we were not able to obtain reliable photometry from the affected data.

Several images were taken with the telescopes properly focussed, in order to check for faint stars within the defocussed PSF of WASP-17. The closest star we detected is 6.9 mag fainter and separated by 69 pixels (27″) from the position of WASP-17. Light from this star did not contaminate any of our observations.

Data reduction was performed as in previous papers (Southworth et al. 2009a,b), using a pipeline written in IDL[2] and calling the DAOPHOT package (Stetson 1987) to perform aperture photometry with the APER[3] routine. The apertures were placed by hand (i.e., mouse-click) and were shifted to follow the positions of the PSFs by cross-correlating each image against a reference image. We tried a wide range of aperture sizes and retained those which gave photometry with the lowest scatter compared to a fitted model. In line with previous experience, we find that the shape of the light curve is very insensitive to the aperture sizes.

Differential photometry was obtained against an optimal en-

semble formed from between two and four comparison stars. Simultaneously to optimisation of the comparison star weights, we fitted low-order polynomials to the out-of-transit data in order to normalise them to unit flux. A first-order polynomial (straight line) was used when possible – such a function is preferable as it is incapable of modifying the shape of the transit – but a second-order polynomial was needed for the third transit to cope with slow variations induced by the changing airmass.

The final light curves have scatters in the region 0.5 mmag per point, which is close to the best achieved at this (or any other) 1.5 m telescope (Southworth et al. 2009c, 2010). They are shown individually in Fig. 1 and tabulated in Table 2.

3 LIGHT CURVE ANALYSIS

The analysis of our light curves was performed identically to the *Homogeneous Studies* approach established by the first author. Full details can be found in Southworth (2008, 2009, 2010, 2011). Here we restrict ourselves to a summary of the analysis steps.

The light curves were modelled using the JKTEBOP[4] code (Southworth et al. 2004a,b). The star and planet are represented by biaxial spheroids, and their shape governed by the mass ratio. We adopted the value 0.0004, but our results are extremely insensitive to this number. The salient parameters of the model are the fractional radii of the star and planet (i.e. absolute radii divided by semimajor axis) r_A and r_b, and the orbital inclination, i. The fractional radii were parameterised by their sum and ratio:

$$r_A + r_b \qquad k = \frac{r_b}{r_A} = \frac{R_b}{R_A}$$

as the latter are less strongly correlated.

3.1 Orbital period determination

Our first step was to obtain a refined orbital ephemeris. Our own four datasets were fitted individually and their errorbars rescaled to give $\chi_\nu^2 = 1.0$ with respect to the best-fitting model. This step is necessary because the uncertainties from our data reduction pipeline (specifically the APER algorithm) tend to be underestimated. We then re-derived the times of mid-transit for the three datasets which covered complete transits. Monte Carlo simulations were used to assess the uncertainties of the measurements, and the resulting errorbars were doubled based on previous experience (Southworth et al. 2012a,b).

We augmented our three times of mid-transit with 13 measurements from A10, of which 12 are from observations with Super-WASP (Pollacco et al. 2006) and one is from their follow-up Euler

---

[2] The acronym IDL stands for Interactive Data Language and is a trademark of ITT Visual Information Solutions. For further details see http://www.ittvis.com/ProductServices/IDL.aspx.

[3] APER is part of the ASTROLIB subroutine library distributed by NASA. For further details see http://idlastro.gsfc.nasa.gov/.

[4] JKTEBOP is written in FORTRAN77 and the source code is available at http://www.astro.keele.ac.uk/jkt/codes/jktebop.html
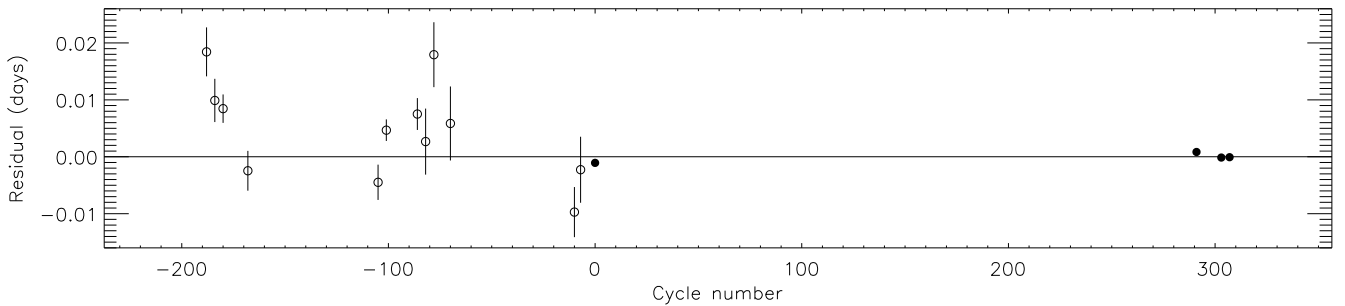
Figure 2. Plot of the residuals of the timings of mid-transit of WASP-17 versus a linear ephemeris. Some error bars are smaller than the symbol sizes. Timings obtained from SuperWASP data are plotted using open circles, and other timings (Danish and Euler telescopes) are plotted with filled circles.

Table 3. Times of minimum light of WASP-17 and their residuals versus the ephemeris derived in this work.
References: (1) A10; (2) This work.

Time of minimum (HJD − 2400000)	Cycle no.	Residual (HJD)	Reference
53890.54887 ± 0.00430	-188.0	0.01843	1
53905.48227 ± 0.00380	-184.0	0.00989	1
53920.42277 ± 0.00250	-180.0	0.00846	1
53965.23767 ± 0.00350	-168.0	-0.00246	1
54200.57117 ± 0.00310	-105.0	-0.00449	1
54215.52227 ± 0.00190	-101.0	0.00468	1
54271.55737 ± 0.00280	-86.0	0.00751	1
54286.49447 ± 0.00580	-82.0	0.00267	1
54301.45167 ± 0.00570	-78.0	0.01793	1
54331.32347 ± 0.00650	-70.0	0.00585	1
54555.43697 ± 0.00440	-10.0	-0.00972	1
54566.65087 ± 0.00580	-7.0	-0.00227	1
54592.80046 ± 0.00038	0.0	-0.00107	1
55679.82838 ± 0.00046	291.0	0.00084	2
55724.65322 ± 0.00056	303.0	-0.00013	2
55739.59522 ± 0.00028	307.0	-0.00007	2

light curve (Table 3). Taking the time of this follow-up dataset as the reference epoch, we find the ephemeris:

$$T_0 = \mathrm{BJD(TDB)}\ 2\,454\,592.80154(50)\ +\ 3.7354845(19) \times E$$

where E represents the cycle count with respect to the reference epoch. The reduced χ^2 of the fit to the timings is rather large at $\chi^2_\nu = 2.37$, and this has been accounted for in the errorbars above. The dominant contribution to this χ^2_ν arises from the SuperWASP timings, which confirms the caveat from A10 that these may have optimistic errorbars.

A plot of the residuals of the fit (Fig. 2) at first sight suggests the possibility of transit timing variations as might arise from the light-time effect induced by a body on a wider orbit around WASP-17 Ab, but a periodogram of the residuals from Table 3 does not show any peaks above the noise level. We therefore proceeded under the reasonable assumption that the orbital period is constant.

3.2 Orbital eccentricity

As emphasised in Sect. 1, the possibility of an eccentric orbit is an important consideration for WASP-17. The radial velocity measurements of the star do not strongly constrain eccentricity; the radial velocity curve of the star has an amplitude not much greater than the size of the errorbars on the individual measurements.

The observed shape of the transit is not useful because it covers only a very small phase interval (an essentially ubiquitous situation for TEPs; see Kipping 2008). The only precise constraint on orbital shape was obtained by A11, from two occultations observed using *Spitzer*. They found the phase of mid-occultation to be 0.50224 ± 0.00050, allowing a detection of a non-zero $e \cos \omega$ at the 4.8σ level.

Our revised period is 4.0 ± 0.6 s larger than that found by A11, a difference of 6.6σ, which affects the phase of mid-occultation. The actual occultation times are not given by A11, but an effective time can be inferred from the dates of the observations and the orbital ephemerides utilised. We performed this calculation and then converted the result back into orbital phase using our new ephemeris. This procedure incorporates the necessary conversion from the UTC to the TDB timescales. We found the phase of occultation to be 0.50066, which is consistent with phase 0.5 at about the 1σ level. The *Spitzer* results can no longer be taken as evidence of an eccentric orbit in the WASP-17 system. This emphasises the importance of accompanying occultation measurements with transits, in order to avoid uncertainties in propagating ephemerides from different observing seasons.

To confirm this result, we obtained a time measurement which represents the actual times of the *Spitzer* occultations by repeating the analysis by A11. We found 2454949.5422 ± 0.0016 on the HJD(UTC) timescale. After converting to the TDB timescale this equates to the phase 0.50059 ± 0.00043, which is equivalent to an $e \cos \omega$ of only 0.00093 ± 0.00068. This differs from zero at the 1.4σ level, which we do not regard as convincing evidence of orbital eccentricity (see also Anderson et al. 2012). Further observations with Warm *Spitzer* would be useful in confirming the phase of mid-occultation of WASP-17 b.

3.3 Light curve modelling

We modelled the three complete transits from the Danish Telescope simultaneously using the JKTEBOP code. The partially-observed transit provides a confirmation of the transit depth, but is less reliable than the other ones and has little effect on the solution, so was not included in further analysis. The χ^2_ν of the fit to the three light curves is 1.22, which indicates that they don't agree completely on the transit shape. Such a situation may arise from astrophysical effects such as starspot activity (which can cause changes in the transit depth without altering the shape), instrumental effects such as correlated noise in the photometry, and analysis effects such as imperfect transit normalisation. Importantly, our possession of three independent transits mitigates against all three eventualities, making the resulting solutions much more reliable than those based on a

Table 4. Parameters of the fit to the light curves of WASP-17 from the JKTEBOP analysis (top lines). The parameters adopted as final are given in bold. Alternative parameters with various constraints on orbital eccentricity and orientation are included, labelled with the $e\cos\omega$ value adopted. The parameters found by other studies are shown in the lowest part of the table. Quantities without quoted uncertainties were not given by those authors, but have been calculated from other parameters which were. $e\cos\omega$ and $e\sin\omega$ values are given to show explicitly the measurements or assumptions relevant to each analysis.

| Source	$e\cos\omega$	$e\sin\omega$	$r_{\rm A}+r_{\rm b}$	k	i (°)	$r_{\rm A}$	$r_{\rm b}$
Danish data	0.0 assumed	0.0 assumed	0.1616 ± 0.0021	0.1255 ± 0.0007	86.71 ± 0.30	0.1436 ± 0.0018	0.01802 ± 0.00030
Euler data	0.0 assumed	0.0 assumed	0.1744 ± 0.0080	0.1322 ± 0.0012	85.46 ± 0.83	0.1540 ± 0.0069	0.0204 ± 0.0011
Danish data	0.036 ± 0.033	-0.10 ± 0.13	0.180 ± 0.023	0.1254 ± 0.0007	85.9 ± 1.1	0.160 ± 0.021	0.0200 ± 0.0026
Danish data	0.00352 ± 0.00075	-0.027 ± 0.019	0.1576 ± 0.0040	0.1254 ± 0.0007	86.87 ± 0.30	0.1400 ± 0.0035	0.01757 ± 0.00047
Danish data	0.00093 ± 0.00068	-0.027 ± 0.019	0.1591 ± 0.0045	0.1255 ± 0.0007	86.81 ± 0.32	0.1414 ± 0.0040	0.01774 ± 0.00054
Adopted solution	0.0 assumed	0.0 assumed	0.1616 ± 0.0021	0.1255 ± 0.0007	$\mathbf{86.71\pm0.30}$	$\mathbf{0.1436\pm0.0018}$	$\mathbf{0.01802\pm0.00030}$
A10 (Case 1)	$0.036^{+0.034}_{-0.031}$	-0.10 ± 0.13	0.1446	$0.1293^{+0.0011}_{-0.0014}$	$87.8^{+2.0}_{-1.0}$	0.1281	0.01658
A10 (Case 2)	$0.034^{+0.025}_{-0.024}$	$-0.233^{+0.071}_{-0.070}$	0.1275	$0.1294^{+0.0010}_{-0.0011}$	$88.16^{+0.58}_{-0.45}$	0.1129	0.01459
A10 (Case 3)	0.0 assumed	0.0 assumed	0.1622	$0.1295^{+0.0010}_{-0.0010}$	$87.8^{+2.0}_{-1.0}$	0.1436	0.01855
Triaud et al. (2010)	0.0 assumed	0.0 assumed	0.1657	$0.12929^{+0.00077}_{-0.00061}$	$86.63^{+0.39}_{-0.45}$	$0.1467^{+0.0033}_{-0.0025}$	$0.01897^{+0.00051}_{-0.00040}$
A11	$0.00352^{+0.00076}_{-0.00073}$	$-0.027^{+0.019}_{-0.015}$	0.1605	0.1302 ± 0.0010	$86.83^{+0.68}_{-0.56}$	0.1420	0.01847
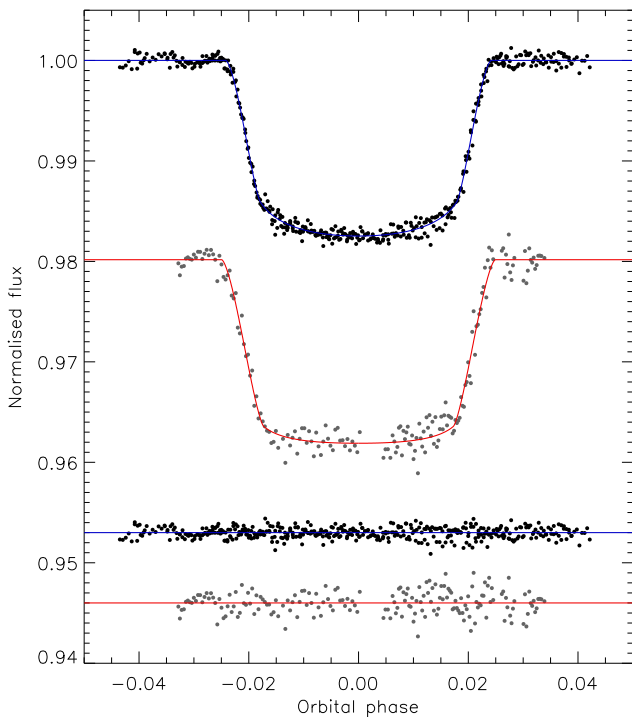
Figure 3. Phased light curves of WASP-17 from the Danish telescope (upper) and the Euler telescope (lower), compared to the best fits found using JKTEBOP and the quadratic LD law. The residuals of the fits are plotted at the bottom of the figure, offset from zero.

single transit. The excess χ^2_ν causes larger errorbars to be obtained for both error anlysis algorithms (see below) so is accounted for in our final results.

Light curve models were obtained using each of five limb darkening (LD) laws, of which four are biparametric (see Southworth 2008). The LD coefficients were either fixed at theoretically predicted values[5] or included as fitted parameters. We found that fitting for one LD coefficient provided a significant im-

provement on fixing both to their theoretical counterparts, but that fitting for both led to ill-conditioned models with no further improvement in the quality of fit. We therefore adopted the fits with the linear LD coefficient fitted and the nonlinear LD coefficient set to its theoretical value but perturbed by ±0.05 on a flat distribution during the error analyses (corresponding to case 'LD-fit/fix' in the nomenclature of Southworth 2011). This does not cause a significant dependence on stellar theory because the two LD coefficients are very strongly correlated (Southworth et al. 2007a). The results for the linear LD law were not used as linear LD is known to be a poor representation of reality.

Errorbars for the fitted parameters were obtained in two ways: from 1000 Monte Carlo simulations for each solution, and via a residual-permutation algorithm. We found that the residual-permutation method returned larger uncertainties for k but not for other parameters, indicating that red noise becomes important when measuring the transit depth. The final parameter values are the unweighted mean of those from the solutions involving the four two-parameter LD laws. Their errorbars are the larger of the Monte-Carlo or residual-permutation alternatives, with an extra contribution to account for variations between solutions with the different LD laws.

We also modelled the Cousins I-band light curve from the Euler Telescope presented by A10, in order to provide a direct comparison with our results. The LD-fit/fix option was also the best, and correlated noise was found to be important for all photometric parameters. A plot of the best fit is shown in Fig. 3 and the corresponding parameters are tabulated in Table 4. The agreement between the Danish and Euler data is poor, especially for k. The Danish results should be more reliable as they are based on three transits obtained using an equatorially-mounted telescope in excellent photometric conditions. The Euler data are more scattered, cover only one transit with a gap near midpoint, and were obtained from an alt-az telescope so suffer from continual changes in the light path over the duration of the observing sequence. We therefore adopted the Danish results as final.

Table 4 also shows a comparison between our photometric pa-

---

[5] Theoretical limb darkening coefficients were obtained by bilinear in-

terpolation in stellar $T_{\rm eff}$ and $\log g$ using the JKTLD code available from http://www.astro.keele.ac.uk/jkt/codes/jktld.html

Table 5. Derived physical properties of the WASP-17 system. The upper part of the table contains the individual results from this work; in each case $g_b = 3.16 \pm 0.20\,\mathrm{m\,s^{-2}}$, $\rho_A = 0.324 \pm 0.012\,\rho_\odot$ and $T'_{eq} = 1755 \pm 28\,\mathrm{K}$.

	(dEB constraint)	(*Claret* models)	(Y^2 models)	(*Teramo* models)	(*VRSS* models)	(*DSEP* models)
$K_b\,(\mathrm{km\,s^{-1}})$	148.38 ± 3.72	148.71 ± 2.88	148.85 ± 1.78	149.78 ± 0.41	148.52 ± 1.49	145.89 ± 2.26
$M_A\,(\mathrm{M_\odot})$	1.272 ± 0.096	1.280 ± 0.076	1.284 ± 0.046	1.308 ± 0.011	1.275 ± 0.038	1.209 ± 0.056
$R_A\,(\mathrm{R_\odot})$	1.577 ± 0.045	1.580 ± 0.040	1.582 ± 0.029	1.592 ± 0.022	1.578 ± 0.027	1.550 ± 0.033
$\log g_A$ (cgs)	4.147 ± 0.015	4.148 ± 0.014	4.148 ± 0.011	4.151 ± 0.011	4.148 ± 0.011	4.140 ± 0.012
$M_b\,(\mathrm{M_{Jup}})$	0.473 ± 0.035	0.475 ± 0.033	0.476 ± 0.029	0.482 ± 0.027	0.474 ± 0.028	0.457 ± 0.029
$R_b\,(\mathrm{R_{Jup}})$	1.925 ± 0.058	1.929 ± 0.052	1.931 ± 0.040	1.943 ± 0.033	1.927 ± 0.038	1.893 ± 0.043
$\rho_b\,(\rho_{Jup})$	0.0620 ± 0.0049	0.0619 ± 0.0048	0.0618 ± 0.0047	0.0614 ± 0.0046	0.0620 ± 0.0046	0.0631 ± 0.0048
Θ	0.0197 ± 0.0012	0.0197 ± 0.0012	0.0196 ± 0.0012	0.0195 ± 0.0011	0.0197 ± 0.0011	0.0200 ± 0.0012
a (AU)	0.05105 ± 0.00128	0.05116 ± 0.00099	0.05121 ± 0.00061	0.05153 ± 0.00014	0.05110 ± 0.00051	0.05019 ± 0.00078
Age (Gyr)		$2.9^{+0.3}_{-1.0}$	$2.7^{+0.4}_{-0.4}$	$2.1^{+0.0}_{-0.1}$	$2.5^{+0.2}_{-1.2}$	$3.3^{+0.6}_{-0.5}$

Table 6. Final physical properties of the WASP-17 system (with statistical and systematic errorbars) compared to published measurements. Eccentricity is included to illustrate the difference approaches taken to obtain each set of results.

	This work (final)	A10 (Case 1)	A10 (Case 2)	A10 (Case 3)	Triaud et al. (2010)	A11
e	0.0 adopted	$0.129^{+0.106}_{-0.068}$	$0.237^{+0.068}_{-0.069}$	0.0 adopted	0.0 adopted	$0.028^{+0.015}_{-0.018}$
$M_A\,(\mathrm{M_\odot})$	$1.286 \pm 0.076 \pm 0.020$	1.20 ± 0.12	1.16 ± 0.12	1.25 ± 0.13	1.20 ± 0.12	1.306 ± 0.026
$R_A\,(\mathrm{R_\odot})$	$1.583 \pm 0.040 \pm 0.008$	$1.38^{+0.20}_{-0.18}$	$1.200^{+0.081}_{-0.080}$	1.566 ± 0.073	$1.579^{+0.067}_{-0.060}$	1.572 ± 0.056
$\log g_A$ (cgs)	$4.149 \pm 0.014 \pm 0.002$	4.23 ± 0.12	4.341 ± 0.068	$4.143^{+0.032}_{-0.031}$		4.161 ± 0.026
$\rho_A\,(\rho_\odot)$	0.324 ± 0.012	$0.45^{+0.23}_{-0.15}$	$0.67^{+0.16}_{-13}$	$0.323^{+0.035}_{-0.028}$	$0.304^{+0.016}_{-0.020}$	0.336 ± 0.030
$M_b\,(\mathrm{M_{Jup}})$	$0.477 \pm 0.033 \pm 0.005$	$0.490^{+0.059}_{-0.056}$	$0.496^{+0.064}_{-0.060}$	$0.498^{+0.059}_{-0.056}$	$0.453^{+0.043}_{-0.035}$	0.486 ± 0.032
$R_b\,(\mathrm{R_{Jup}})$	$1.932 \pm 0.052 \pm 0.010$	$1.74^{+0.26}_{-0.23}$	1.51 ± 0.10	1.97 ± 0.10	$1.986^{+0.089}_{-0.074}$	1.991 ± 0.081
$g_b\,(\mathrm{m\,s^{-2}})$	3.16 ± 0.20	$3.63^{+1.4}_{-0.9}$	$5.0^{+1.1}_{-0.9}$	$2.92^{+0.36}_{-0.33}$		2.81 ± 0.27
$\rho_b\,(\rho_{Jup})$	$0.0618 \pm 0.0048 \pm 0.0003$	$0.092^{+0.054}_{-0.032}$	$0.144^{+0.042}_{-0.031}$	$0.0648^{+0.0106}_{-0.0090}$		0.0616 ± 0.0080
T'_{eq} (K)	1755 ± 28	1662^{+113}_{-110}	1557 ± 55	1756^{+26}_{-30}		1771 ± 35
Θ	$0.0196 \pm 0.0012 \pm 0.0001$					
a (AU)	$0.05125 \pm 0.00099 \pm 0.00027$	$0.0501^{+0.0017}_{-0.0018}$	$0.0494^{+0.0017}_{-0.0018}$	$0.0507^{+0.0017}_{-0.0018}$	0.0500 ± 0.0017	0.05150 ± 0.00034
Age (Gyr)	$2.7^{+0.6}_{-1.0}{}^{+0.6}_{-0.6}$	$3.0^{+0.9}_{-2.6}$	$1.2^{+2.8}_{-1.2}$	$3.1^{+1.1}_{-0.8}$		2.65 ± 0.25

rameters and those published by other researchers. The values from Triaud et al. (2010) and A11 are in good agreement with our results, except for the parameter k. This is as expected, because those authors had only the Euler light curve with which to constrain the transit shape. The parameters from A10 are more discrepant, primarily because their favoured solution is for a large orbital eccentricity.

To demonstrate the influence of eccentricity, we have rerun the above analyses on the Danish data for three eccentric orbits, applying constraints using the method described by Southworth et al. (2009c). For the first set of constraints we used $e\cos\omega = 0.036 \pm 0.033$ and $e\sin\omega = -0.10 \pm 0.13$ (A10), for the second we adopted $e\cos\omega = 0.00352 \pm 0.00075$ and $e\sin\omega = -0.027 \pm 0.019$ (A11), and for the third we specified $e\cos\omega = 0.00093 \pm 0.00068$ and $e\sin\omega = -0.027 \pm 0.019$ (Sect. 3.2).

The results for these three alternative sets of constraints are shown in Table 4. It can be seen that k is unaffected but, as expected, $r_A + r_b$ and thus r_A and r_b are very dependent on the treatment of eccentricity. That large eccentricities can be ruled out is vital for precisely measuring the properties of WASP-17. The very small $e\cos\omega$ value allowed by the transit and occultation timings (Sect. 3.2) results in photometric parameters which are close to the 1σ errorbars of the zero-eccentricity result, and illustrates the small change in the measured system properties to be expected if the 1.4σ measurement of $e\cos\omega$ turns out to be real.

4   THE PHYSICAL PROPERTIES OF WASP-17

The physical properties of the WASP-17 system can be obtained from the adopted photometric parameters (Table 4), the orbital velocity amplitude of the star ($K_A = 52.7 \pm 2.9\,\mathrm{m\,s^{-1}}$; Triaud et al. 2010), its effective temperature (T_{eff}) and metallicity ($\left[\frac{Fe}{H}\right]$), and a constraint from theoretical stellar evolutionary models. Full details of our approach can be found in Southworth (2009, 2010).

One immediate problem faced here is the diversity of the published T_{eff} measurements of WASP-17 A: A10 find $6550 \pm 100\,\mathrm{K}$ from analysis of échelle spectra; Triaud et al. (2010) obtain $6650 \pm 80\,\mathrm{K}$ from similar observations, and Maxted et al. (2011) deduce $6500 \pm 75\,\mathrm{K}$ from the InfraRed Flux Method (IRFM; Blackwell & Shallis 1977; Blackwell et al. 1980). We adopted $T_{eff} = 6550 \pm 100\,\mathrm{K}$ as this encompasses all three determinations but leans towards the IRFM value, which should be the method with the least dependence on stellar theory and analysis technique. The corresponding metallicity is $\left[\frac{Fe}{H}\right] = -0.25 \pm 0.09$ (A10).

Our approach was to guess a value of the orbital velocity of the planet (K_b) and combine it with the photometric parameters and K_A to calculate the physical properties of both bodies using standard formulae (e.g. Hilditch 2001). The predicted properties of the star for the calculated mass were then found via interpolation in a set of theoretical model predictions. K_b was iteratively adjusted to find the best agreement between the known r_A and calculated $\frac{R_A}{a}$, and between the measured and predicted T_{eff} values. This was done

Table 7. Compilation of selected physical properties of TEP systems containing a planet larger than $1.6\,\mathrm{R_{Jup}}$. The projected spin-orbit misalignment measurable from the Rossiter-McLaughlin effect is denoted by λ. All asymmetric errorbars have been averaged, and the statistical and systematic errorbars have been added in quadrature, in order to fit into the Table.
References: (1) Hartman et al. (2011); (2) Hartman et al. (2012); (3) Latham et al. (2010); (4) Southworth (2012); (5) Fortney et al. (2011); (6) Konacki et al. (2005); (7) Southworth (2010); (8) Konacki et al. (2003); (9) Snellen et al. (2009); (10) Mandushev et al. (2007); (11) Hebb et al. (2009); (12) Joshi et al. (2009); (13) Enoch et al. (2011).

System	M_A ($\mathrm{M_\odot}$)	R_A ($\mathrm{R_\odot}$)	T_{eff} (K)	$\left[\frac{\mathrm{Fe}}{\mathrm{H}}\right]$	e	Period (d)	M_b ($\mathrm{M_{Jup}}$)	R_b ($\mathrm{R_{Jup}}$)	T'_{eq} (K)	λ (°)	$\log R'_{\mathrm{HK}}$	Refs
HAT-P-32	1.160 ±0.041	1.219 ±0.016	6207 ±88	-0.04 ±0.08	0.0	2.150	0.860 ±0.164	1.789 ±0.025	1786 ±26			1
HAT-P-33	1.375 ±0.040	1.637 ±0.034	6446 ±88	$+0.07$ ±0.08	0.0	3.475	0.762 ±0.101	1.686 ±0.045	1782 ±28			1
HAT-P-40	1.512 ±0.073	2.206 ±0.061	6080 ±100	$+0.22$ ±0.10	0.0	4.457	0.615 ±0.038	1.730 ±0.062	1770 ±33		-5.12	2
HAT-P-41	1.418 ±0.047	1.683 ±0.047	6390 ±100	$+0.21$ ±0.10	0.0	2.694	0.800 ±0.102	1.685 ±0.064	1941 ±38		-5.04	2
Kepler-7	1.41 ±0.10	2.028 ±0.038	5933 ±50	$+0.11$ ±0.05	0.0	4.885	0.453 ±0.068	1.649 ±0.038	1619 ±15		-5.099	3,4
Kepler-12	1.16 ±0.12	1.490 ±0.050	5947 ±100	$+0.07$ ±0.04	0.0	4.438	0.430 ±0.049	1.695 ±0.030	1485 ±25			5,4
OGLE-TR-10	1.277 ±0.083	1.520 ±0.100	6075 ±86	$+0.28$ ±0.10	0.0	3.101	0.68 ±0.15	1.706 ±0.054	1702 ±54			6,7
OGLE-TR-56	1.34 ±0.10	1.737 ±0.045	6119 ±62	$+0.25$ ±0.08	0.0	1.212	1.41 ±0.18	1.734 ±0.059	2482 ±30			8,4
OGLE-TR-L9	1.43 ±0.10	1.499 ±0.043	6933 ±58	-0.05 ±0.20	0.0	2.486	4.4 ±1.5	1.633 ±0.046	2034 ±22			9,4
TrES-4	1.339 ±0.086	1.834 ±0.087	6200 ±75	$+0.14$ ±0.09	0.0	3.554	0.897 ±0.075	1.735 ±0.072	1805 ±40	$+6.3 \pm 4.7$	-5.104	10,4
WASP-12	1.38 ±0.19	1.619 ±0.079	6300 ±100	$+0.30$ ±0.10	$0.018^{+0.024}_{-0.014}$	1.091	1.43 ±0.14	1.825 ±0.094	2523 ±45		-5.500	11,4
WASP-14	1.35 ±0.12	1.666 ±0.087	6475 ±100	$+0.0$ ±0.2	0.088 ±0.003	2.244	7.90 ±0.47	1.633 ±0.092	2090 ±59	-33.1 ± 7.4	-4.923	12,4
WASP-17	1.286 ±0.079	1.583 ±0.041	6550 ±100	-0.25 ±0.09	0.0	3.735	0.477 ±0.033	1.932 ±0.053	1755 ±28	$-148.5^{+4.2}_{-5.4}$	-5.331	This work
WASP-48	1.19 ±0.05	1.75 ±0.09	6000 ±150	-0.12 ±0.12	0.0	2.144	0.98 ±0.09	1.67 ±0.10	2030 ±70			13

for ages ranging from zero to the point at which the star evolves to $\log g < 3.5$, leading to a final set of best-fitting physical properties and age for the system.

Statistical errors in the input parameters were propagated using a perturbation analysis (Southworth et al. 2005). Systematic errors arising from the use of theoretical predictions were estimated by running separate solutions for each of five independent stellar model tabulations: *Claret* (Claret 2004), Y^2 (Demarque et al. 2004), *Teramo* (Pietrinferni et al. 2004), *VRSS* (VandenBerg et al. 2006) and *DSEP* (Dotter et al. 2008). Finally, a model-independent set of results was generated using an empirical calibration of stellar properties found from well-studied eclipsing binaries, a process we label "dEB constraint". The empirical calibration follows the approach introduced by Enoch et al. (2010) but with the improved calibration coefficients derived by Southworth (2011).

The results for each approach are given in Table 5. The mass, radius, surface gravity and density of the star are denoted by M_A, R_A, $\log g_A$ and ρ_A, and of the planet by M_b, R_b, g_b and ρ_b. The orbital semimajor axis is a, T'_{eq} is the equilibrium temperature of the planet (neglecting albedo and heat redistribution) and Θ is the Safronov (1972) number. We find that the agreement between the model sets is excellent except for the *DSEP* models, which are quite discrepant. Southworth (2011) noticed that the agreement between models deteriorates at lower metallicities, as is experienced here. Our final physical properties for the WASP-17 system (Table 6)

were therefore calculated from the results obtained using the other four model sets (*Claret*, Y^2, *Teramo* and *VRSS*). Table 6 also contains results from published studies of WASP-17, which are in good agreement overall but contain some optimistic errorbars.

5 WHAT CAUSES SUCH LARGE PLANET RADII?

We have measured the radius of WASP-17 b to be $R_b = 1.932 \pm 0.053\,\mathrm{R_{Jup}}$ (adding the statistical and systematic errors in quadrature), confirming its status as the largest planet currently known. We also find no significant evidence for orbital eccentricity, removing an additional contribution to the uncertainties of the measured properties of the system.

Its closest competitor, HAT-P-32 b, suffers a similar problem concerning the influence of orbital shape on the resulting planetary radius (Hartman et al. 2011). However, in its case the possibilities are switched because the eccentric-orbit alternative has a positive $e \sin \omega$ compared to the previously-postulated negative $e \sin \omega$ for WASP-17. The preferred solution for HAT-P-32, with a circular orbit, results in a smaller radius ($R_b = 1.789 \pm 0.025\,\mathrm{R_{Jup}}$) compared to the eccentric-orbit alternative ($R_b = 2.037 \pm 0.099\,\mathrm{R_{Jup}}$ with $e = 0.163 \pm 0.061$).

The other twelve TEPs with radii above $1.6\,\mathrm{R_{Jup}}$ are listed in Table 7 with a summary of the physical properties of them and
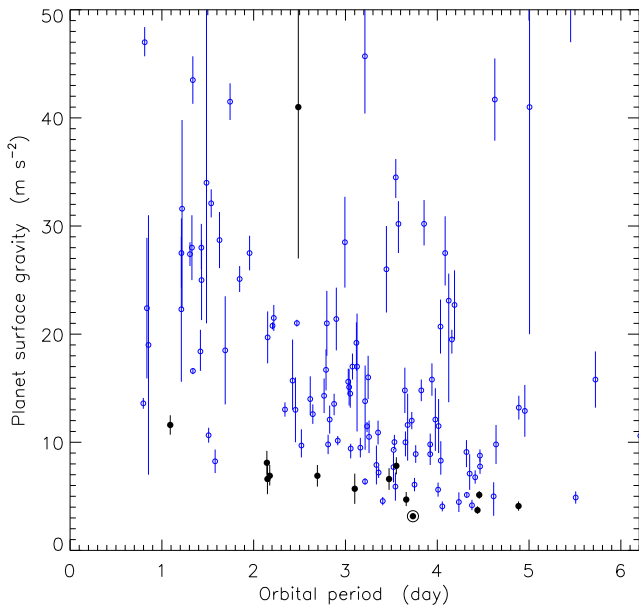
Figure 4. Plot of orbital period versus surface gravity for the known transiting planets. Planets with radii above $1.6\,R_{\rm Jup}$ are shown using black filled circles, and WASP-17 b is highlighted with an extra circle. The other planets are shown with lighter open circles.

Figure 5. Plot of stellar $T_{\rm eff}$ versus planet radius for the known transiting systems. Other comments are the same as in Fig.4.

their parent stars. This list has been boosted by the addition of two objects, OGLE-TR-56 and WASP-14, based on major revisions to their radii by Southworth (2012). The newly-discovered systems WASP-78 and WASP-79 (Smalley et al. 2012) are not included here as the radii of their planets are uncertain. We now discuss the properties of the fourteen planets with radii above $1.6\,R_{\rm Jup}$.

Firstly, Fig. 4 shows that their orbital period distribution[6] is not exceptional, and that they are consistent with the known correlation between period and surface gravity (Southworth et al. 2007b). The masses of all but two of them (OGLE-TR-L9 and WASP-12) are in the interval 0.4–$1.0\,M_{\rm Jup}$. These objects also do not represent a high-eccentricity population: all have orbits which are (or are almost) circular[7]. Tidal heating (Bodenheimer et al. 2001; Jackson et al. 2008; Ibgui & Burrows 2009) is therefore not a viable proposition to explain their large radii. Orbital misalignment may be relevant: WASP-14 is misaligned (Johnson et al. 2009), WASP-17 is retrograde (Triaud et al. 2010), and TrES-4 is axially aligned (Narita et al. 2010). Thus two of the three planets with obliquity measurements are misaligned.

However, a noticable feature of the fourteen large planets is that they orbit host stars with $T_{\rm eff} > 5900\,{\rm K}$ and $M_{\rm A} > 1.15\,M_{\odot}$. This establishes a connection between a bloated planet and a hot star. Fig. 5 and Fig. 6 show that the large planets are preferentially associated with hotter and more massive host stars. The association does not work the other way: such stars also possess TEPs with smaller radii representative of the general planet population. A correlation with host star $\left[\frac{\rm Fe}{\rm H}\right]$ was suspected but not found. An important factor in bloating planets above their expected size therefore seems to be the $T_{\rm eff}$ of their host star. This may be due to the enhanced UV flux from such stars, but such a possibility does not explain why less inflated planets are found around stars with $T_{\rm eff} > 5900\,{\rm K}$.

A similar situation occurs with irradiation: the large planets have high $T_{\rm eq}'$s (or equivalently large specific incident stellar fluxes) of 1600 K or more, but so do many other smaller planets. The connection between inflated radii and high $T_{\rm eq}'$ is well-known (see Baraffe et al. 2010; Enoch et al. 2012, and references therein) but the simultaneous existence of small planets with high $T_{\rm eq}'$ is not yet understood. Laughlin et al. (2011) quantified the correlation between the radius anomaly (observed radius versus those predicted by the models of Bodenheimer et al. 2003) of TEPs and their $T_{\rm eq}'$s, in the form of a power law. Whilst their fig. 2 exhibits appreciable evidence for this claim, the large planets discussed here remain outliers even in that diagram.

We have searched for values for the chromospheric activity indicator $\log R_{\rm HK}'$ (Noyes et al. 1984) for the host stars of our large planets. Knutson et al. (2010) give values of -5.331 for WASP-17, -5.099 for Kepler-7, -5.104 for TrES-4, -5.500 for WASP-12 and -4.923 for WASP-14. These $\log R_{\rm HK}'$ values are representative of inactive stars, suggesting a correlation between inflated planetary radii and low chromospheric activity. HAT-P-32 and HAT-P-33 possess values of the related S index (Vaughan et al. 1978) which indicate a low activity level, despite their comparatively high rotation rates and velocity jitter (Hartman et al. 2011). HAT-P-40 and HAT-P-41 have similarly quiet $\log R_{\rm HK}'$ values of -5.12 and -5.04 (Hartman et al. 2012).

Therefore eight of the fourteen stars in question have measured activity indicators, and all suggest low chromospheric activity. Perhaps the increased high-energy photon flux from more active stars acts against large planetary radii. Knutson et al. (2010) found a correlation with the atmospheric properties of planets, in that inactive stars possess planets with temperature inversions whereas planets around active stars do not have inversions. However, Hartman (2010) found no correlation between $\log R_{\rm HK}'$ and

---

[6] Data taken from the Transiting Extrasolar Planet Catalogue (TEPCat), available at: http://www.astro.keele.ac.uk/jkt/tepcat/

[7] It has been noticed that orbital eccentricity is correlated with planet mass (Southworth et al. 2009c) but plots of planet radius versus eccentricity (not shown here) indicate that there is – if anything – a deficit of large-radius eccentric planets.
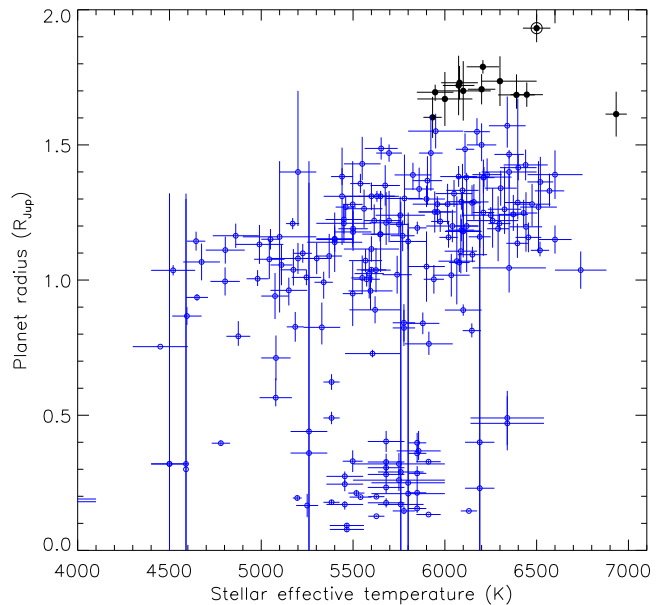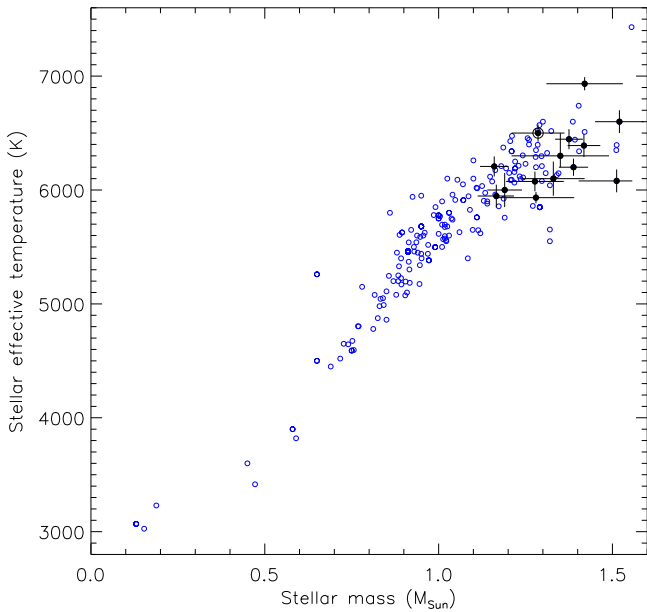
Figure 6. Plot of stellar mass versus effective temperature for the known transiting planets (data taken from TEPCat). Other comments are the same as in Fig.4. The errorbars of the planets have been surpressed for clarity, with the exception of those fourteen with a large radius.

Figure 7. Plot of stellar versus planet radius for the known TEP systems. Other comments are the same as in Fig.4. Points without errorbars represent those discovered via the space telescopes CoRoT and *Kepler*, whose discovery biases are very different from those of ground-based surveys.

planet radius, so the low values for the fourteen host stars in question may be an artefact of their T_{eff} distribution.

Another possibility to explain the large planetary radii is that the more massive stars, around which the larger planets are found, have shorter main-sequence lifetimes. They will therefore be on average younger than the less massive TEP host stars. The large planets could simply be at an earlier stage of their evolution. This is, however, at odds with the low activity levels of the host stars, which implies that they are not particularly young. The models by Fortney et al. (2007, their fig. 5) show that it is possible for planets to be $2.0\,\mathrm{R_{Jup}}$ or above if they are young (of order 10^7 yr) and low-mass (less than $1\,\mathrm{M_{Jup}}$). These criteria are not satisfied by any of our large planets. Explaining the radii of the large TEPs is therefore only viable if there is a large systematic error in our estimation of the age of their host stars, which is unlikely but certainly not impossible.

5.1 Can observational biases explain the properties of large planets?

An important question is whether the correlation between large planets and hot and massive host stars is real, or is it merely a phantom arising from observational selection effects? The correlation could easily be suspected to arise from detection biases as a function of transit depth. Fig. 7 shows a plot of the radii of the host stars versus their planets. We have overlaid dotted lines to indicate loci of approximately constant transit depth, calculated using JKTEBOP and assuming quadratic LD with both coefficients equal to 0.30. The subset of planets discovered via space telescopes are down-played in Fig. 7, as these should be much less biased against finding systems with shallow transits. It is immediately clear that the large planets do not stand out in this diagram as having unusually deep, and therefore easily detectable, transits.

Fig. 7 shows that most known TEPs have transit depths of about 1–3%. Firstly, we are straightforwardly biased against find-
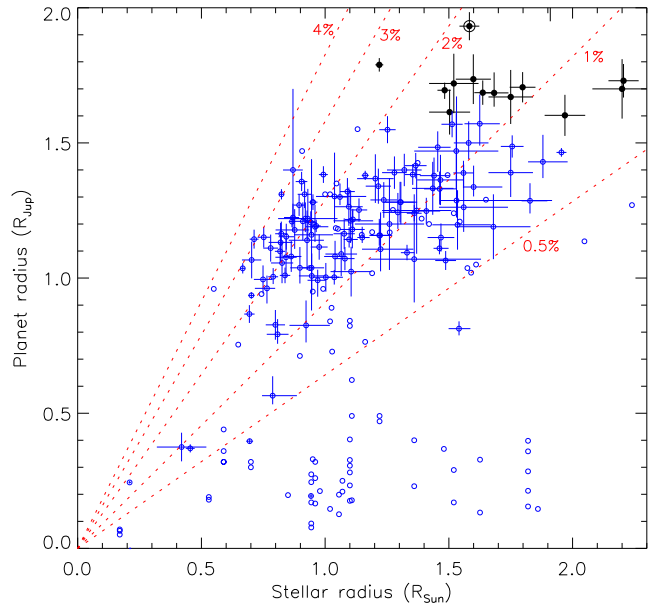
ing small planets around hotter (and therefore bigger) stars, as the transit depths in these systems are small. The relative paucity of small planets around big stars is plausibly explained by lower detection probabilities for transits less than 0.5% deep. Secondly, the absence of large planets around small stars might be explicable by either natural rarity or a bias against deep transits. Such objects may have a low follow-up priority within planet-search consortia if it is believed that deep transits are associated with false positives such as eclipsing binary star systems. As an example, if WASP-17 b orbited an unevolved $0.9\,\mathrm{M_\odot}$ star then the transit depth would be roughly 5%.

None of the observables discussed above pre-determines the existence of big planets. They are found only around hotter stars, but some such stars possess small planets. They have quite high T'_{eq}s, but so do many smaller planets. They do not give rise to unusually deep or shallow transits, which rules out the more simple observational biases, and the metallicities of their host stars are not exceptional. The question of what causes their bloated radii remains unsettled.

6 SUMMARY AND CONCLUSIONS

Whilst WASP-17 was widely regarded to be the largest known planet, its radius was uncertain as it was based primarily on one follow-up transit light curve which shows moderate correlated noise. In this work we present three new high-precision transit light curves, obtained using telescope-defocussing techniques, and improve the measurement of its radius.

We have refined the orbital ephemeris of the system using our new data, which increase the temporal baseline by 3.1 years. Our revised orbital period is 4.0 ± 0.6 s longer than previous measurements, a difference of 6.6σ, and this change is sufficient to bring the observed time of occultation (A11) into line with that expected for a circular orbit. Further observations would allow this result to

be checked. In the case of WASP-17, circularity of the orbit favours a larger value for the planetary radius.

We have modelled our new data, along with the single follow-up light curve presented in the discovery paper (A10), using the JKTEBOP code. We paid careful attention to the treatment of limb darkening and to obtaining reliable uncertainties. The physical properties of the system were then derived using our new photometric and published spectroscopic results. Remaining uncertainties and discrepancies in the existing $T_{\rm eff}$ and $\left[\frac{\rm Fe}{\rm H}\right]$ measurements of the host star impose a bottleneck on the quality of the resulting properties, and new radial velocity observations would also be useful in refining the measurement of the planet's mass and therefore its density.

WASP-17 b is the largest known planet, with a radius of $R_{\rm b} = 1.932 \pm 0.053\,{\rm R_{Jup}}$. Another eleven planets are known with radii greater than $1.6\,{\rm R_{Jup}}$. They are found only around comparatively hot ($T_{\rm eff} > 5900\,{\rm K}$) and massive ($M_{\rm A} > 1.15\,{\rm M_\odot}$) stars, and have correspondingly high equilibrium temperatures ($T'_{\rm eq} > 1600\,{\rm K}$ with the exception of Kepler-12) and equivalently incident fluxes. But other stars of similar mass and $T_{\rm eff}$ possess smaller planets, whilst other planets with similar $T'_{\rm eq}$ (or equivalently specific incident flux) do not have such enlarged radii. One possible discriminating feature is that all eight of the fourteen host stars with measured activity indicators are chromospherically inactive.

The set of fourteen large planets do not have unusual transit depths. However, planets of this size around cooler stars may have an anomalously low discovery rate if their deep transits (of order 5%) discount them from detailed follow-up observations. High-precision radial velocity measurements are expensive in terms of telescope time, so dubious TEP candidates with unexpectedly deep transits may be prematurely rejected as false positives. A re-evaluation of such objects will either yield scientifically valuable discoveries, or dismiss the existence of large planets around small stars.

The fourteen planets with radii greater than $1.6\,{\rm R_{Jup}}$ all have circular (or nearly circular) orbits, so their large size cannot easily be attributed to tidal heating. Of the three published measurements of the axial alignments of these planets, one reveals a retrograde orbit, one a misaligned orbit, and one indicates alignment. Observations of the Rossiter-McLaughlin effect on the remaining eleven systems could either verify or discount the possibility that axial alignment is a relevant aspect of large planets.

ACKNOWLEDGMENTS

REFERENCES

Adams, E. R., et al., 2011, ApJ, 741, 102
Anderson, D. R., et al., 2010, ApJ, 709, 159
Anderson, D. R., et al., 2011, MNRAS, 416, 2108
Anderson, D. R., et al., 2012, MNRAS, 422, 1988
Baraffe, I., Chabrier, G., Barman, T., 2010, Reports on Progress in Physics, 73, 016901
Bayliss, D. D. R., Winn, J. N., Mardling, R. A., Sackett, P. D., 2010, ApJ, 722, L224
Blackwell, D. E., Shallis, M. J., 1977, MNRAS, 180, 177
Blackwell, D. E., Petford, A. D., Shallis, M. J., 1980, A&A, 82, 249
Bodenheimer, P., Lin, D. N. C., Mardling, R. A., 2001, ApJ, 548, 466
Bodenheimer, P., Laughlin, G., Lin, D. N. C., 2003, ApJ, 592, 555
Claret, A., 2004, A&A, 424, 919
Collier Cameron, A., et al., 2010, MNRAS, 407, 507
Demarque, P., Woo, J.-H., Kim, Y.-C., Yi, S. K., 2004, ApJS, 155, 667
Dotter, A., Chaboyer, B., Jevremović, D., Kostov, V., Baron, E., Ferguson, J. W., 2008, ApJS, 178, 89
Doyle, L. R., et al., 2011, Science, 333, 1602
Enoch, B., Collier Cameron, A., Parley, N. R., Hebb, L., 2010, A&A, 516, A33
Enoch, B., Collier Cameron, A., Horne, K., 2012, A&A, 540, A99
Enoch, B., et al., 2011, AJ, 142, 86
Fortney, J. J., Marley, M. S., Barnes, J. W., 2007, ApJ, 659, 1661
Fortney, J. J., et al., 2011, ApJS, 197, 9
Gillon, M., et al., 2007, A&A, 466, 743
Hartman, J. D., 2010, ApJ, 717, L138
Hartman, J. D., et al., 2011, ApJ, 742, 591
Hartman, J. D., et al., 2012, AJ submitted, arXiv:1207.3344
Hebb, L., et al., 2009, ApJ, 693, 1920
Hébrard, G., et al., 2010, A&A, 516, A95
Hellier, C., et al., 2009, Nature, 460, 1098
Hilditch, R. W., 2001, An Introduction to Close Binary Stars, Cambridge University Press, Cambridge, UK
Ibgui, L., Burrows, A., 2009, ApJ, 700, 1921
Jackson, B., Greenberg, R., Barnes, R., 2008, ApJ, 681, 1631
Johnson, J. A., Winn, J. N., Albrecht, S., Howard, A. W., Marcy, G. W., Gazak, J. Z., 2009, PASP, 121, 1104
Joshi, Y. C., et al., 2009, MNRAS, 392, 1532
Kipping, D. M., 2008, MNRAS, 389, 1383
Knutson, H. A., Howard, A. W., Isaacson, H., 2010, ApJ, 720, 1569
Konacki, M., Torres, G., Jha, S., Sasselov, D. D., 2003, Nature, 421, 507
Konacki, M., Torres, G., Sasselov, D. D., Jha, S., 2005, ApJ, 624, 372
Kopal, Z., 1959, Close binary systems, The International Astrophysics Series, London: Chapman & Hall, 1959
Latham, D. W., et al., 2010, ApJ, 713, L140
Laughlin, G., Crismani, M., Adams, F. C., 2011, ApJ, 729, L7
Léger, A., et al., 2009, A&A, 506, 287

Lissauer, J. J., et al., 2011, Nature, 470, 53

Lucy, L. B., Sweeney, M. A., 1971, AJ, 76, 544

Mandushev, G., et al., 2007, ApJ, 667, L195

Maxted, P. F. L., Koen, C., Smalley, B., 2011, MNRAS, 418, 1039

Narita, N., Sato, B., Hirano, T., Winn, J. N., Aoki, W., Tamura, M., 2010, PASJ, 62, 653

Noyes, R. W., Hartmann, L. W., Baliunas, S. L., Duncan, D. K., Vaughan, A. H., 1984, ApJ, 279, 763

Pietrinferni, A., Cassisi, S., Salaris, M., Castelli, F., 2004, ApJ, 612, 168

Pollacco, D. L., et al., 2006, PASP, 118, 1407

Safronov, V. S., 1972, Evolution of the Protoplanetary Cloud and Formation of the Earth and Planets (Jerusalem: Israel Program for Scientific Translation)

Smalley, B., et al., 2012, A&A submitted, `arXiv:1206.1177`

Snellen, I. A. G., et al., 2009, A&A, 497, 545

Southworth, J., 2008, MNRAS, 386, 1644

Southworth, J., 2009, MNRAS, 394, 272

Southworth, J., 2010, MNRAS, 408, 1689

Southworth, J., 2011, MNRAS, 417, 2166

Southworth, J., 2012, MNRAS, submitted

Southworth, J., Maxted, P. F. L., Smalley, B., 2004a, MNRAS, 349, 547

Southworth, J., Maxted, P. F. L., Smalley, B., 2004b, MNRAS, 351, 1277

Southworth, J., Maxted, P. F. L., Smalley, B., 2005, A&A, 429, 645

Southworth, J., Bruntt, H., Buzasi, D. L., 2007a, A&A, 467, 1215

Southworth, J., Wheatley, P. J., Sams, G., 2007b, MNRAS, 379, L11

Southworth, J., Bruni, I., Mancini, L., Gregorio, J., 2012a, MNRAS, 420, 2580

Southworth, J., Mancini, L., Maxted, P. F. L., Bruni, I., Tregloan-Reed, J., Barbieri, M., Ruocco, N., Wheatley, P. J., 2012b, MNRAS, 422, 3099

Southworth, J., et al., 2009a, MNRAS, 396, 1023

Southworth, J., et al., 2009b, MNRAS, 399, 287

Southworth, J., et al., 2009c, ApJ, 707, 167

Southworth, J., et al., 2010, MNRAS, 408, 1680

Stetson, P. B., 1987, PASP, 99, 191

Triaud, A. H. M. J., et al., 2010, A&A, 524, A25

VandenBerg, D. A., Bergbusch, P. A., Dowler, P. D., 2006, ApJS, 162, 375

Vaughan, A. H., Preston, G. W., Wilson, O. C., 1978, PASP, 90, 267

Winn, J. N., et al., 2011, ApJ, 737, L18

Wood, P. L., Maxted, P. F. L., Smalley, B., Iro, N., 2011, MNRAS, 412, 2376